

Global surface warming enhanced by weak Atlantic overturning circulation

Xianyao Chen¹ & Ka-Kit Tung^{2*}

Evidence from palaeoclimatology suggests that abrupt Northern Hemisphere cold events are linked to weakening of the Atlantic Meridional Overturning Circulation (AMOC)¹, potentially by excess inputs of fresh water². But these insights—often derived from model runs under preindustrial conditions—may not apply to the modern era with our rapid emissions of greenhouse gases. If they do, then a weakened AMOC, as in 1975–1998, should have led to Northern Hemisphere cooling. Here we show that, instead, the AMOC minimum was a period of rapid surface warming. More generally, in the presence of greenhouse-gas heating, the AMOC's dominant role changed from transporting surface heat northwards, warming Europe and North America, to storing heat in the deeper Atlantic, buffering surface warming for the planet as a whole. During an accelerating phase from the mid-1990s to the early 2000s, the AMOC stored about half of excess heat globally, contributing to the global-warming slowdown. By contrast, since mooring observations began^{3–5} in 2004, the AMOC and oceanic heat uptake have weakened. Our results, based on several independent indices, show that AMOC changes since the 1940s are best explained by multidecadal variability⁶, rather than an anthropogenically forced trend. Leading indicators in the subpolar North Atlantic today suggest that the current AMOC decline is ending. We expect a prolonged AMOC minimum, probably lasting about two decades. If prior patterns hold, the resulting low levels of oceanic heat uptake will manifest as a period of rapid global surface warming.

As an analogy of the flow of energy in our climate system, consider the filling of a bucket of water from a tap at the top. The feed rate of the tap is an analogue of the top-of-atmosphere radiative imbalance—the net heating—of our planet, with the water level in the bucket analogous to surface warming. The sink at the bucket bottom drains into a larger bucket below (the deeper oceans). If the drain rate is the same as the feed rate from the tap at the top, the water level in the bucket does not rise (hiatus of surface warming). If the drain is plugged, the water level will rise rapidly in the bucket (rapid surface warming). AMOC controls about half of the variation of this ‘drain rate’.

Figure 1 quantifies the energy budget of our climate system, using the subsurface ocean heat content (OHC) measured mostly by a system of autonomous profiling Argo floats, during a period, 2000–2014, when the ‘drain rate’ was large. The total OHC, as approximated by that in the upper 1,500 m of the oceans, is increasing at a rate of about $0.42 \pm 0.02 \text{ W m}^{-2}$, consistent with radiative imbalance⁷. The upper 200 m roughly corresponds to the mixed layer globally. Through wind and turbulent mixing, variations of sea surface temperature (SST) and mixed-layer OHC are highly statistically correlated ($r = 0.82$ in 13-month running mean). Figure 1 shows that both were in a warming slowdown for this period. Why the upper 200 m OHC was in a warming slowdown is clear: the increase in heat storage below 200 m, about 89 zettajoules ($1 \text{ ZJ} = 10^{21} \text{ J}$). This amount of heat is equivalent to 180 years of the world’s energy consumption at the current rate, and any future variation even within this observed range will have important consequences for the surface temperature.

If the radiative imbalance and the heat storage below 200 m were to remain the same, the 0–1,500 m OHC would still increase at the same rate as the radiative imbalance, but the 0–200 m OHC curve would lie on the 0–1,500 m curve, increasing at the same rate, or about 0.23°C per decade. Our best estimate for the next two decades, allowing for some increase in ocean storage, is 70% of that rate, at 0.16°C per decade (see Methods), close to the 25-year trend of 0.177°C per decade of the last rapid warming period in the twentieth century⁸.

The inset of Fig. 1 shows how the global increase in OHC storage between 200 m and 1,500 m are partitioned among the various oceans. The Pacific and the Indian oceans dominate the horizontal exchanges of heat in the upper 300 m^{9,10}, and the Atlantic and the Southern oceans dominate the vertical redistribution¹¹. They accounted for about 70% of the global heat storage increase in the 200–1,500 m layer during 2000–2014, divided between the North Atlantic, which is dominant before 2005, and the Southern Ocean after 2005. The subsurface warming in the Southern Ocean started in 1993 according to the data available (see below), and was attributed to the southward displacement and intensification of the circumpolar jet⁸, caused in large part by the Antarctic ozone hole¹². The North Atlantic’s role appears to be cyclic on decadal timescales, with AMOC in an accelerating phase before 2005.

AMOC transports warm saline surface water found in the subtropical Atlantic to the subpolar Atlantic, where heat loss to the cold atmosphere increases its density. Aided by its high salinity it sinks and returns southward at depth. When AMOC is stronger (weaker), more (less) of the warm and saline water is found in the subpolar Atlantic, and subsequent sinking subducts more (less) heat there, as demonstrated in Fig. 2. The contrast is dramatic between periods when AMOC is increasing and when it is decreasing. Why AMOC sometimes accelerates or declines is more complicated. It could be responding to external forcing, for example, such as the freshening of the subpolar waters from melting ice at the end of the Little Ice Age¹³. Or, AMOC could be part of a natural, multidecadal variability involving feedbacks between the density effect of salinity on deep convection in Labrador and the Nordic Seas, and the subsequent induced northward transport of surface salinity reinforcing the deep convection¹⁴.

AMOC is commonly believed to be slowing on centennial timescales owing to global warming. The RAPID/MOCHA mooring array, deployed in 2004³ off the coast of Florida to monitor AMOC, soon afterwards recorded its weakening⁴. The decadal decline, however, is ten times larger than the predicted forced response⁵, causing concerns about its long-term trend and possible deficiencies of the models used. Figure 3a, constructed from various independent proxies from 1945 to the present (see Extended Data Fig. 1 for unfiltered time series and Extended Data Fig. 2 for error bars), shows that it is dominated instead by reversing phases. The weakening AMOC, by 3.7 Sverdrups (Sv) since 2005 measured by the RAPID/MOCHA array, was actually preceded by an acceleration^{15,16}. Altimetry data of sea-surface heights (SSH) available since 1993¹⁷ were used to deduce¹⁸ via geostrophic balance that at 41°N AMOC sped up by 4 Sv from the early 1990s to 2005, consistent with Zhang’s subsurface fingerprint proxy⁶. We use multiple

¹Physical Oceanography Laboratory, CIMST, Ocean University of China, and Qingdao National Laboratory of Marine Science and Technology, Qingdao, China. ²Department of Applied Mathematics, University of Washington, Seattle, WA, USA. *e-mail: ktung@uw.edu

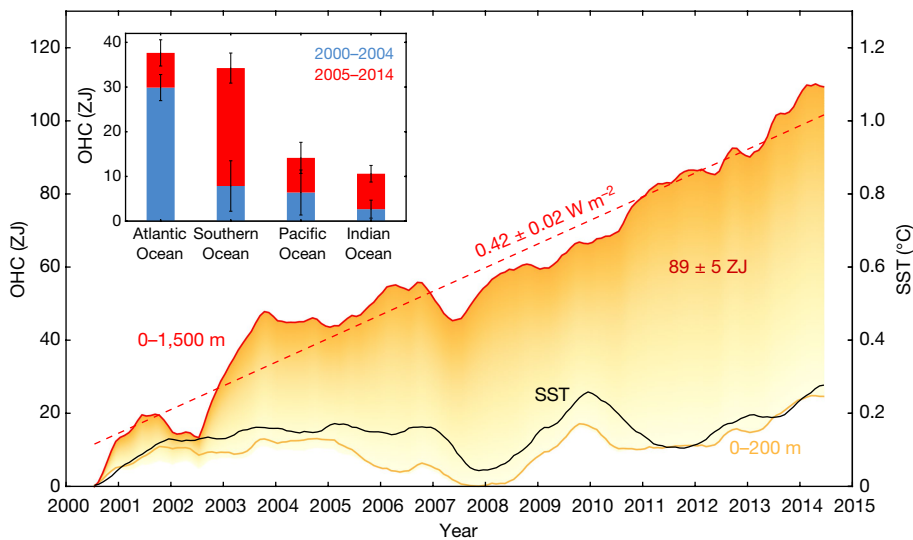


Fig. 1 | Quantifying the global heat budget and the partition among ocean basins in the two periods 2000–2004 and 2005–2014. The SST from ERSST.v4 is shown as a black curve and the 0–200-m OHC from the ISHII and Scripps datasets (see Methods) is shown as an orange curve, showing that they co-vary and that both are in a warming slowdown, while the total OHC, as approximated by the 0–1,500-m OHC (red curve), is increasing at the regressed linear rate of $0.42 \pm 0.02 \text{ W m}^{-2}$ (red dashed straight line). This excess heat from forcing is sequestered below 200 m. The orange-shaded region represents the additional amount of heat stored in the 200–1,500 m layer since 2000, about 89 ZJ. One zettajoule

independent proxies to infer subpolar AMOC strength back in time to 1945. Many of the proxies used here have been validated by models: Zhang's subsurface temperature fingerprint was highly coherent with AMOC strength^{6,19,20} at low frequencies in the model (GFDL CM2.1) at mid-latitudes. The subpolar gyre SST proxy²¹, and the upper ocean subpolar salinity proxy²⁰ were also model-validated. Along with the long record of tide gauges along the east coast of the USA²², these proxies

is equivalent to twice the world's annual energy consumption. If this additional storage were absent, the upper 200 m would have increased at the rapid rate of the red curve. We adjusted the data for the Southern Ocean to remove a possible artefact due to the rapid transition from no-Argo to the Argo observing platform around 2002–2003²⁸. The inset shows the division of the 89 ZJ of global ocean increase in heat storage in the 200–1,500 m layer into the four ocean basins and two periods. 35° S marks the northern boundary of the Southern Ocean and the southern boundary of the Atlantic, Pacific and Indian oceans. The error bars are one-standard-deviation errors of the linear regression.

consistently indicate a period of low AMOC from the mid-1970s to the 1990s. The shading in Fig. 3 shows that this period coincided with a period of rapid surface warming. See also Extended Data Fig. 3 for the coincidence of Atlantic OHC change and global surface warming. See Methods for model–observation reconciliation.

We call AMOC+ (AMOC-) the phase when the AMOC strength is above (below) climatology (based on the subpolar salinity, which has

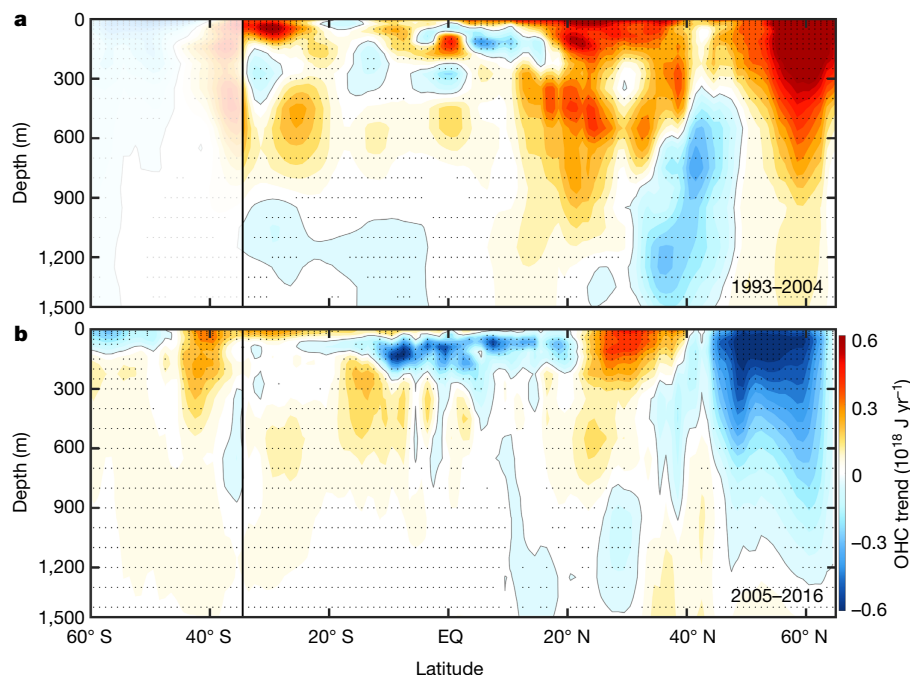


Fig. 2 | The OHC linear trend in the Atlantic basin. The trend is zonally averaged over two periods, when AMOC is increasing (a) and decreasing (b). The two periods are chosen according to the observed AMOC trends in Fig. 3a. ISHII data are used in the first period and Scripps data are used

in the second period. Stippling indicates areas of statistical significance at the 95% confidence level. The linear trend is unreliable in the Southern Ocean prior to 2005, and so that region is masked.

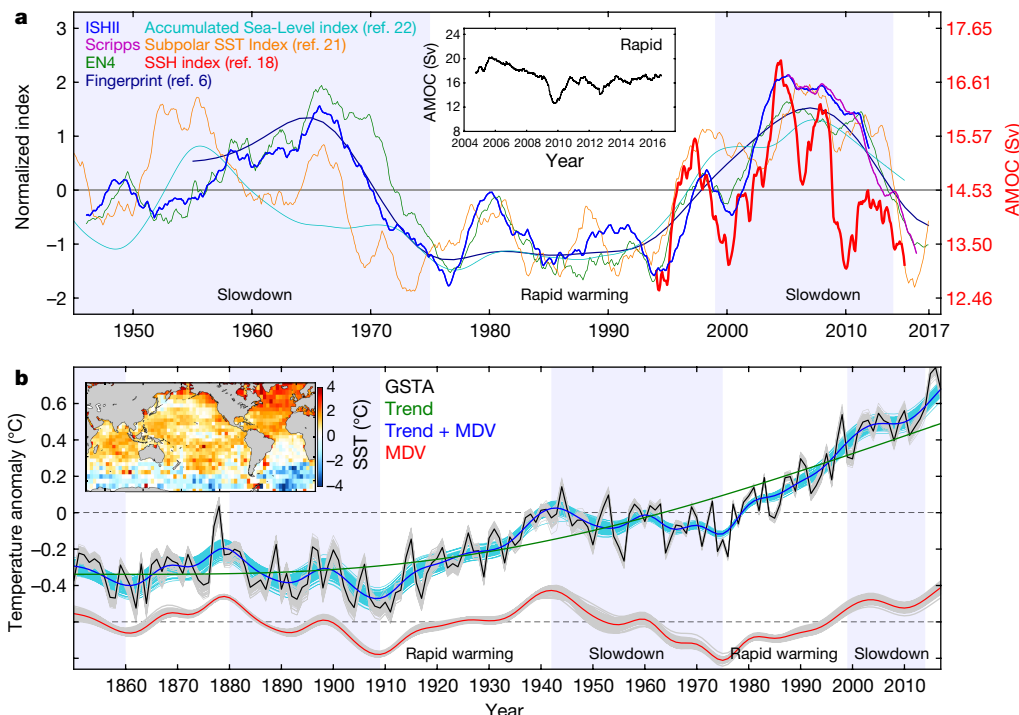


Fig. 3 | AMOC and GSTA variations. **a**, Mid and subpolar latitude AMOC strength, as calculated at 41° N using altimetry measurements, from ref. ¹⁸ (red, two-year running mean, Sverdrup scale shown on the right); inferred from integrated subpolar salinity in 0–1,500 m and 45–65° N in the Atlantic as a proxy, using the ISHII (dark blue) and Scripps (purple) datasets, with a two-year running mean. The green curve is the subpolar salinity, similarly calculated but using EN4. The AMOC fingerprint⁶ (dark blue) and the accumulated sea-level index (turquoise) calculated from historical tide gauge measurements²² were smoothed with 10-year and 7-year low-pass filters, respectively, from their sources. The subpolar gyre

SST index²¹ in orange is also a two-year running mean. See Methods for details. The inset shows RAPID-measured AMOC at 26° N. **b**, Shown are GSTA from HadCRUT4.6 (black), the nonlinear secular trend (close to the 100-year linear trend) (brown) and variation about the trend for timescales longer than decadal (multidecadal variability (MDV), red). The inset shows the SST spatial pattern associated with MDV obtained by regressing SST onto its time series. The blue curve is the smoothed version of GSTA obtained as the sum of the secular trend and MDV. The faint lines around the solid lines are from 100 ensemble members of the HadCRUT4.6, which assess the range of uncertainty of the data used in the solid lines.

a long record with no trend). The high (+) phase consists of two rapid subphases. The increasing subphase (AMOC_{up}) started in 1993, from the low point in AMOC_- , first slowly and then rapidly, peaking in 2005. It is then followed by a rapid decreasing subphase ($\text{AMOC}_{\text{down}}$) (2005 to the present) (Fig. 3a). At low values of overturning (AMOC_-) the strength is relatively level even though there are short-term fluctuations, because a slower poleward transport of saline water from the tropical Atlantic makes it difficult to speed up the sinking in the subpolar North Atlantic except through slower processes: The surface water could slowly become more saline through the reduction of fresh water outflow from land glaciers and from the Arctic Ocean²³. The northward transport of warm and saline water increased more rapidly since 1999, and started a negative feedback as the warm surface water increased glacier melt and freshwater outflow. The previous $\text{AMOC}_{\text{down}}$ subphase of 1965–1974 started with the gradual freshening of the north Atlantic waters, as can be inferred from the decreasing salinity in the subpolar region, braking the AMOC. Incidentally, both SSH at 41° N and RAPID at 26° N showed a simultaneous, short-lived 30% drop in AMOC strength in 2009–2010⁵, partially caused by an extreme negative episode of atmospheric North Atlantic Oscillation that affected the wind field⁵ over both areas.

Water masses in the subpolar and subtropical gyres are different and transports across gyre boundaries need not be continuous¹⁴. For vertical heat subduction, it is mainly the subpolar AMOC that is our focus in Fig. 3a. Signals from salinity proxies at the subpolar Atlantic have almost reached the previous low. The subpolar gyre SST has started to warm. The deep Labrador Sea density, which is known to lead by 7–10 years changes in wider basin AMOC^{15,16}, has stopped declining since 2014 (Extended Data Fig. 4). The subtropical region is more prone to higher-frequency perturbations¹⁴, and the RAPID time series is

experiencing its short-term oscillations (two so far) after the recovery from the large dip in 2010 so the decadal trend may be difficult to see. Nevertheless, it appears to have stabilized at that latitude. Previously, when AMOC reached its lowest AMOC_- value after 1975, that level phase lasted two and a half decades. Although we have data only for one cycle, its observed non-sinusoidal pattern characterized by a prolonged flat minimum separated by steep peaks is as expected from the physical arguments presented above.

The longer Global-mean Surface Temperature Anomaly (GSTA) record shown in Fig. 3b, together with its low-frequency variation^{24,25}, consists of a secular trend and a multidecadal variability (MDV), defined to be on timescales that are decadal or longer. The spatial pattern associated with MDV (inset to Fig. 3b) has the pattern of an interhemispheric seesaw in the Atlantic, with the North Atlantic being the centre of action, consistent with model results²⁶. When the MDV is increasing it doubles the GSTA warming rate over the 100-year trend of 0.08 K per decade, and is associated with a period of rapid warming in the late and also the early twentieth century. That secular trend of 0.08 K per decade, statistically significant at over 95% confidence level against a second-order autoregressive (AR(2)) red noise, has been attributed to the underlying anthropogenic global warming trend²⁷. The regressed spatial pattern associated with the secular trend resembles the model-predicted response from greenhouse warming^{24,25}. The MDV in the GSTA is related to the Atlantic Multidecadal Oscillation (AMO) (see Methods), the latter having a record extending back several hundred years.

The previous period of low overturning in the AMOC—phase, from 1975 to the 1990s, coincided with a period of rapid global warming at the surface. This is more than a coincidence because the energy budget involved can be quantified. We do not have reliable subsurface data for

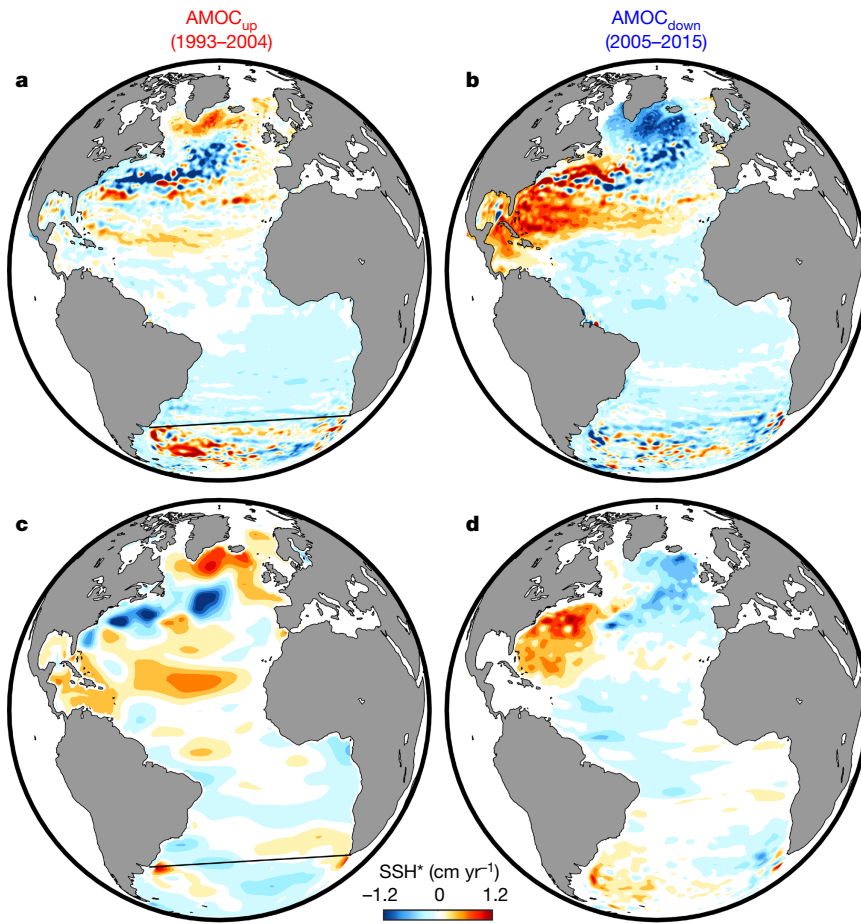


Fig. 4 | Contrasting thermosteric SSH* patterns for increasing and decreasing AMOC. **a, c**, Linear SSH* trend when AMOC is increasing; **b, d**, Linear SSH* trend when AMOC is decreasing. **a** and **b** show SSH*

the period when the surface warming was rapid. However, the change from that period can be quantified so that an estimate can be made for what would happen if that change were absent. During 2000–2005, in the AMOC_{up} subphase, 52% of the global increase between 200 m and 1,500 m is sequestered in the Atlantic. Together with the heat sequestered in the Southern Ocean, it contributed to a period of global warming slowdown. When this additional heat storage is absent, a period of rapid surface warming is expected to reoccur.

Although the Argo programme was launched around 2000, its coverage in the Southern Ocean did not become adequate until 2005. To validate the data on OHC we compare satellite SSH* (the asterisk indicates the deviation of SSH from its global mean) available since 1993 (Fig. 4a and b) to the thermosteric sea level rise (due to thermal expansion of the water column) (Fig. 4c and d) calculated using OHC above 1,500 m. The comparison is surprisingly good north of 35° S. Notable exceptions are as expected; they include areas with no Argo measurements: shallow maritime areas west of the Caribbean islands, and the deep mid-Atlantic Ocean below 1,500 m, which was not included in our OHC. South of 35° S the linear trend in the Argo data is not reliable across 2003 during the transition from no-Argo to Argo measurements²⁸. The two datasets consistently show that in the subpolar Atlantic there is increasing (decreasing) heat storage when AMOC is increasing (decreasing). The southward (northward) displacement of the Gulf Stream at mid-latitudes created some compensating cooling (warming)²¹. In the AMOC's rapidly decreasing subphase, some heat is entrained in the subtropical gyre. The Southern Hemisphere north of 35° S is mostly featureless. South of 35° S, mesoscale patterns of warming can be seen in SSH*, which is also reflected in the OHC after 2004, but not before, owing to data quality. These mesoscale eddies in the linear trend

from remote sensing, compared with the steric sea level calculated using OHC in **c** and **d**. SSH* is SSH with its global mean subtracted, reflecting mostly the thermosteric part of SSH (see Methods).

occurring south of the Antarctic Circumpolar Current may be due to its recent strengthening, and its increased baroclinic instability²⁹.

The increased sea level (Fig. 4b) and warmer SST (Extended Data Fig. 5d) in the western subtropical Atlantic may have led to strong hurricanes and their destructive power, and the surprising string of category-5 hurricanes making landfall towards the end of the decreasing phase of the AMOC, instead of at the peak of the AMOC, when the mean SST of the entire North Atlantic is the warmest and the basin-wide hurricane number is the highest³⁰.

Climate-model runs under preindustrial conditions demonstrated the existence of multidecadal variation in AMOC, and its associated Atlantic SST variation: the AMOC+ (AMOC-) phase corresponds to warm (cold) SST and Northern Hemisphere mean surface temperature^{6,19}. This prevailing paradigm has permeated popular perceptions about the future climate consequence of an AMOC weakened by global warming, similar to the abrupt switch back into icy conditions of the Younger Dryas during the last deglaciation². Over the past few decades, however, there is a positive trend of warmer subsurface water in the subpolar Atlantic (Extended Data Fig. 6), rendering the mean state lighter (see the temperature–salinity diagram in Extended Data Fig. 7). Deep convections can now carry more heat downward. In the presence of greenhouse heating from above and warmer SSTs, AMOC's role in sequestering heat becomes important in the current global surface energy budget (Fig. 1). When AMOC is more constant, as in the AMOC- phase, little additional heat is sequestered in the Atlantic, contributing to a more rapid surface warming as more heat from radiative imbalance remains on the surface and the upper 200 m of the global oceans. We note, however, that we have discussed here only one component of a complex system: global heat balance is maintained by

the combined ocean and atmosphere systems and a change in the transport of one regional component may affect the partitioning of change between other parts of the ocean or of the atmosphere, depending on the timescales involved.

Online content

Any Methods, including any statements of data availability and Nature Research reporting summaries, along with any additional references and Source Data files, are available in the online version of the paper at <https://doi.org/10.1038/s41586-018-0320-y>.

Received: 25 January 2018; Accepted: 6 June 2018;

Published online 18 July 2018.

1. McManus, J. F., Francois, R., Gherardi, J.-M., Keigwin, L. D. & Brown-Leger, S. Collapse and rapid resumption of Atlantic meridional circulation linked to deglacial climate changes. *Nature* **428**, 834–837 (2004).
2. Manabe, S. & Stouffer, R. J. Coupled ocean-atmosphere model response to freshwater input: comparison to Younger Dryas Event. *Paleoceanography* **12**, 321–336 (1997).
3. McCarthy, G. D. et al. Measuring the Atlantic Meridional Overturning Circulation at 26° N. *Prog. Oceanogr.* **130**, 91–111 (2015).
4. Smed, D. A. et al. Observed decline of the Atlantic meridional overturning circulation 2004–2012. *Ocean Sci.* **10**, 29–38 (2014).
5. Srokosz, M. A. & Bryden, H. L. Observing the Atlantic Meridional Overturning Circulation yields a decade of inevitable surprises. *Science* **348**, (2015).
6. Zhang, R. Coherent surface-subsurface fingerprint of the Atlantic meridional overturning circulation. *Geophys. Res. Lett.* **35**, L20705 (2008).
7. Loeb, N. G. et al. Observed changes in top-of-the-atmosphere radiation and upper-ocean heating consistent within uncertainty. *Nat. Geosci.* **5**, 110–113 (2012).
8. Solomon, S. et al. (eds) *Climate Change 2007: the Physical Science Basis. Contribution of Working Group I to the Fourth Assessment Report of the Intergovernmental Panel on Climate Change* (Cambridge Univ. Press, Cambridge, 2007).
9. Lee, S.-K. et al. Pacific origin of the abrupt increase in Indian Ocean heat content during the warming hiatus. *Nat. Geosci.* **8**, 445–449 (2015).
10. Nieves, V., Willis, J. K. & Patzert, W. C. Recent hiatus caused by decadal shift in Indo-Pacific heating. *Science* **349**, 532–535 (2015).
11. Chen, X. & Tung, K. Varying planetary heat sink led to global-warming slowdown and acceleration. *Science* **345**, 897–903 (2014).
12. Thompson, D. W. J. & Solomon, S. Interpretation of recent Southern Hemisphere climate change. *Science* **296**, 895–899 (2002).
13. Thornalley, D. J. R. et al. Anomalously weak Labrador Sea convection and Atlantic overturning during the past 150 years. *Nature* **556**, 227–230 (2018).
14. Lozier, M. S. Overturning in the North Atlantic. *Annu. Rev. Mar. Sci.* **4**, 291–315 (2012).
15. Robson, J., Ortega, P. & Sutton, R. A reversal of climatic trends in the North Atlantic since 2005. *Nat. Geosci.* **9**, 513–517 (2016).
16. Jackson, L. C., Peterson, K. A., Roberts, C. D. & Wood, R. A. Recent slowing of Atlantic overturning circulation as a recovery from earlier strengthening. *Nat. Geosci.* **9**, 518–522 (2016).
17. Beckley, B. D. et al. Assessment of the Jason-2 extension to the TOPEX/Poseidon, Jason-1 sea-surface height time series for global mean sea level monitoring. *Mar. Geodesy* **33**, 447–471 (2010).
18. Willis, J. K. Can in situ floats and satellite altimeters detect long-term change in Atlantic Ocean overturning? *Geophys. Res. Lett.* **37**, <https://doi.org/10.1029/2010GL042372> (2010).
19. Yan, X., Zhang, R. & Knutson, T. R. The role of Atlantic overturning circulation in the recent decline of Atlantic major hurricane frequency. *Nat. Commun.* **8**, (2017).
20. Zhang, R. On the persistence and coherence of subpolar sea surface temperature and salinity anomalies associated with the Atlantic multidecadal variability. *Geophys. Res. Lett.* **44**, 7865–7875 (2017).
21. Caesar, J., Rahmstorf, S., Robinson, A., Feulner, G. & Saba, V. Observed fingerprint of a weakening Atlantic Ocean overturning circulation. *Nature* **556**, 191–196 (2018).
22. McCarthy, G. D. & Haigh, I. D., Hirschi, J. J.-M., Grist, J. P. & Smeed, D. A. Ocean impact on decadal Atlantic climate variability revealed by sea-level observations. *Nature* **521**, 508–510 (2015).
23. Polyakov, I. V. et al. Arctic Ocean freshwater changes over the past 100 years and their causes. *J. Clim.* **21**, 364–384 (2008).
24. Chen, X. & Tung, K. K. Global mean surface temperature variability—space-time perspective from rotated EOFs. *Clim. Dyn.* <https://doi.org/10.1007/s00382-017-3979-0> (2017).
25. Wu, Z., Huang, N. E., Wallace, J. M., Smoliak, B. & Chen, X. On the time-varying trend in global-mean surface temperature. *Clim. Dyn.* **37**, 759–773 (2011).
26. Zhang, R., Delworth, T. L. & Held, I. M. Can the Atlantic Ocean drive the observed multidecadal variability in Northern Hemisphere mean temperature? *Geophys. Res. Lett.* **34**, L02709 (2007).
27. Tung, K. K. & Zhou, J. Using data to attribute episodes of warming and cooling in instrumental records. *Proc. Natl. Acad. Sci. USA* **110**, 2058–2063 (2013).
28. Cheng, L. J. & Zhu, J. Artifacts in variations of ocean heat content induced by the observation system changes. *Geophys. Res. Lett.* **41**, 7276–7283 (2014).
29. Marshall, J. & Speer, K. Closure of the meridional overturning circulation through Southern Ocean upwelling. *Nat. Geosci.* **5**, 171–180 (2012).
30. Yan, X., Zhang, R. & Knutson, T. R. The role of Atlantic Overturning Circulation in the recent decline of Atlantic major hurricane frequency. *Nat. Commun.* **8**, 1695 (2017).

Acknowledgements The research of K.-K.T. is supported by the National Science Foundation, under AGS-1262231 and by the Frederic and Julia Wan Endowed Professorship. X.C. was supported by the National Key Basic Research Program of China under grant 2015CB953900 and by the Natural Science Foundation of China under grants 41330960 and 41776032.

Author contributions K.-K.T. and X.C. undertook the analysis of global ocean temperature and salinity profiles, RAPID observations, and satellite altimetry datasets. K.-K.T. led the draft of this manuscript. X.C. produced all figures. Both authors contributed substantially to the drafting and revision of this manuscript.

Competing interests The authors declare no competing interests.

Additional information

Extended data is available for this paper at <https://doi.org/10.1038/s41586-018-0320-y>.

Reprints and permissions information is available at <http://www.nature.com/reprints>.

Correspondence and requests for materials should be addressed to K.-K.T.

Publisher's note: Springer Nature remains neutral with regard to jurisdictional claims in published maps and institutional affiliations.

METHODS

Updated AMOC indices. We reproduced the unfiltered monthly AMOC indices (Extended Data Fig. 1). Their correlation coefficient with Zhang's unfiltered AMOC fingerprint is listed on the right. All correlations are statistically significant at over 95% confidence level.

AMOC indices in Fig. 3a. Extended Data Fig. 1 shows that all unfiltered AMOC proxies used in Fig. 3a are correlated with Zhang's fingerprint AMOC proxy at over 95% confidence level. Zhang showed²⁰ that in the Geophysical Fluid Dynamics Laboratory model the fingerprint proxy is highly coherent with the model AMOC Index, defined as the zonal integrated maximum Atlantic overturning at 40° N, at decadal and multidecadal scales. This is the reason that the fingerprint is shown smoothed with a 10-year low-pass filter. This fingerprint is calculated using the detrended 400-m subsurface temperature. (It was updated to 2017 by the author with permission to use.)

Our subpolar upper ocean salinity index is defined as the average over 45°–65° N in the Atlantic basin and integrated over 0–1,500 m. The two undetrended salinity indices shown in Fig. 3 and Extended Data Fig. 1 are from three data sources. The first index is based on ISHII and Scripps. ISHII data have not been updated since 2012 and Scripps data are only available since 2004; they are connected at 2012 when calculating the correlation coefficient with Zhang's fingerprint AMOC proxy. The data source for the second salinity index is from EN4 (version 4.2.1).

The sea-level index was obtained as in ref.²² by calculating the sea-level difference between the average of a group of linearly detrended, deseasonalized tide-gauge measurements south of 35° N and that to the north. It is accumulated in time, shifted to the right by 4.8 years and smoothed with a 7-year lowpass filter.

The subpolar gyre SST index was obtained by 'detrending' the subpolar gyre SST by the subtraction of the global mean SST. It is averaged over the subpolar gyre region, defined by ref.²¹.

Willis' AMOC strength at 41° N was calculated¹⁸ using altimetry SSH measurements and geostrophic approximation for the zonal-mean northward velocity vertically integrated above 1,130 m. It is not detrended or accumulated.

Error bars for data used in Fig. 3. The error bars for the salinity time series used in Fig. 3a are plotted in Extended Data Fig. 2. The uncertainty at each gridpoint is provided by each data source: ISHII, Scripps and EN4. The error bar of the salinity time series at each time is computed as the combination of the gridpoint uncertainty and one standard deviation due to the averaging in space. The uncertainty of the SSH-deduced AMOC strength was given by ref.¹⁸. The measurement and sampling errors at each time gridpoint were ±12%. The uncertainty of tide-gauge data was discussed by ref.²², and that of Zhang's fingerprint proxy by ref.³⁰. The uncertainty of the global surface temperature data from HadCRUT4.6 was assessed by the data source using 100 ensemble members that span the uncertainty range of the data.

Calculation of warming scenarios. We emphasize that this is not a prediction, but a scenario calculation. In our current climate system, the OHC in the upper 1,500 m of the global oceans increases at the rate of 0.42 W m⁻², which is approximately the top-of-atmosphere radiative imbalance. Apart from short-term variations of radiative imbalance such as those due to volcanic eruptions, it is reasonable to assume that for the next two decades there will not be an appreciable change in radiative imbalance, barring an unexpected development of carbon sequestration technology.

Scenario 1. If the OHC storage below 200 m remains the same (no increases), then the radiative imbalance of the 0.42 W m⁻² heats only the top 200 m of the global oceans. That is, the increase of OHC in the top 200 m of the column. The top 200 m of the global ocean then warms at the rate calculated as: 0.42 W m⁻² divided by the heat capacity of 200 m of the ocean = 0.23 °C per decade. This is equivalent to that obtained for a 'slab' ocean of 200 m thick.

Scenario 2. As for Scenario 1 except that only the Atlantic and the Southern oceans' heat content below 200 m remain the same for the next two decades. The Pacific and the Indian oceans continue to increase their OHC at the current rate. The warming rate is 70% of that for Scenario 1 because at present the Atlantic and the Southern oceans together are responsible for 70% of the OHC increase in the upper 1,500 m of the oceans. This is probably the more likely scenario because we have argued in the main text that AMOC is likely to remain relatively constant during the next two decades. The subsurface Southern Ocean has been warming since at least 1993, caused by the southward displacement and intensification of the westerly jet, which cannot continue much longer, first because the proposed cause (the ozone hole) has diminished in importance as the ozone hole heals, and second because there is not much more room for the jet's southward displacement. So the increase in warming will probably stop.

Model AMOC and reconciliation with recent observations. Observational results in Fig. 3a show that there was a positive trend from 1993 to 1999, with a small peak in 1996. The rapid rising trend from 1999 to 2005 is statistically significant at the over 95% confidence level. This is seen in all proxies, most clearly in the less

smoothed data (SSH and subpolar salinity). This claim is supported by observation of SSH-deduced AMOC strength, tide-gauges, the subpolar salinity proxy, and also the Zhang fingerprint proxy. (The last proxy, because of 10-year smoothing, does not show the smaller peak in the mid-1990s). A model reanalysis also showed an acceleration prior to 2005 followed by a decline at 26° N, and a peak in the mid-1990s as well as one in 2005 at 45° N¹⁶. AMOC in models is sensitive to resolution and subgrid parameterization³¹, resulting in little consensus among reanalysis (and hindcast) products. With one exception¹⁶ these products do not agree with the RAPID observation at 26° N. The exception is the GloSea5 model, which has a higher, eddy-permitting resolution than previous reanalyses. Supplementary figure 1 of ref.¹⁶ shows two peaks, one at 1995 and one at 2005. The 1995 peak is slightly higher than the 2005 peak, and is referred to thus in the main text of ref.¹⁶: "The AMOC at 45° N is representative of the changes in the subpolar gyre, with the AMOC decreasing from a maximum in the mid-1990s, followed by a slight increase (Fig. 1d)". The peak in 2005 was not mentioned. However, the result on the 1995 peak should be treated with care, as the authors themselves stated in the supplementary information of ref.¹⁶: "It is likely that there will be a period of spinup, where the deep ocean (where there are few observational constraints) adjusts, which may explain the divergence in trend. Hence we disregard the first few years of each experiment. There is also a shock in 1992 when the altimeter data is introduced, which may contribute to the increase in AMOC strength between 1989 and 1995. Hence we choose the period to analyse starting from January 1995, and join the two analyses in January 2002." The relative magnitude of the 1995 peak and the 2005 peak may be unreliable as it was obtained by joining two reanalyses, one starting from 1989 and one from 1995 with "divergence in trend"¹⁶.

The observed SSH data since 1992 can be used to deduce AMOC strength using geostrophic approximation, bypassing the problems of shock and subsequent adjustment when the same SSH data were introduced in model assimilation.

SST changes during different phases of AMOC. The upper branch of the climatological AMOC brings warm and saline surface water from the subtropical North Atlantic to its subpolar latitudes. When the overturning is stronger, more of this warm water is found in the subpolar northern latitudes. In the Southern Hemisphere, more of the cold water from the region of the Antarctic Circumpolar Current is brought northward into the Southern subtropics. Consequently a characteristic signature in the Atlantic SST is an opposite-signed multidecadal anomaly, with warming to the north and smaller cooling to the south when the overturning is stronger (AMOC+), and the reverse pattern when it is weaker (AMOC-) (Extended Data Fig. 5a, b). This ocean-induced SST variability is centered in the subpolar North Atlantic²⁰. The observed tendency during the last two subphases of the AMOC is as expected (Extended Data Fig. 5c, d): As AMOC slows after 2005, the SST tends towards a cooler North Atlantic and warmer subtropics. Accompanying the strong cooling in the subpolar gyre is an interesting intense warming after 2005 in the northwest Atlantic, centered in the Gulf of Maine, which was recently simulated in a high-resolution climate model³² as due to the northward displacement of the Gulf Stream when AMOC slows. The inverse relationship between Gulf Stream's northward displacement and AMOC strength was found⁶ to be caused by the Labrador Current retreat and the bottom vortex stretching³³.

AMO. In long coupled atmosphere-ocean model runs under preindustrial conditions (without increasing greenhouse gases) the AMO is the SST manifestation of AMOC variations, and the two time series are approximately in phase¹⁹. The definition of AMO in ref.¹⁹ is the mean of Atlantic SST north of 45° N, which may lead the subtropical SST anomaly by two years. A more traditional definition of AMO is the mean Atlantic SST north of the Equator³⁴, with an approximately one-year phase difference. It has been shown²⁴, using the space-time perspective of rotated empirical orthogonal function analysis, that the AMO is mainly responsible for the observed global mean surface temperature variation on multidecadal timescales. The two are in phase during the industrial era. Since the AMOC and the global mean surface temperature variation are not in phase (as shown in Fig. 3), it follows that during the industrial era, AMOC and AMO are off phase, possibly by a quarter cycle, although AMOC's time series is too short for an accurate determination of the phase information.

During the positive phase of AMO, SST is warm in the North Atlantic and surrounding continents. Therefore, Northern Hemisphere mean surface temperature is warm during the positive phase and cool during the negative phase of the AMO. Using multiproxy data in the Northern Hemisphere the AMO time series can be extended back several hundred years³⁵. The longest instrumental temperature record exists in central England, and it was used²⁷ to reconstruct the AMO time-series back to the Little Ice Ages. An even longer record of ice cores in Greenland, in the northern Atlantic, exists, and a statistically significant at the over 95% confidence level AMO signal can be found³⁶ extending back to 800 AD that is coherent with the instrumental record of central England²⁷ during their overlapping period. It appears that AMO is a recurrent phenomenon of period around 65–70 years and that it is robust in the preindustrial era, with the Atlantic and the surrounding areas warm during the positive phase and cold during the negative phase. From climate

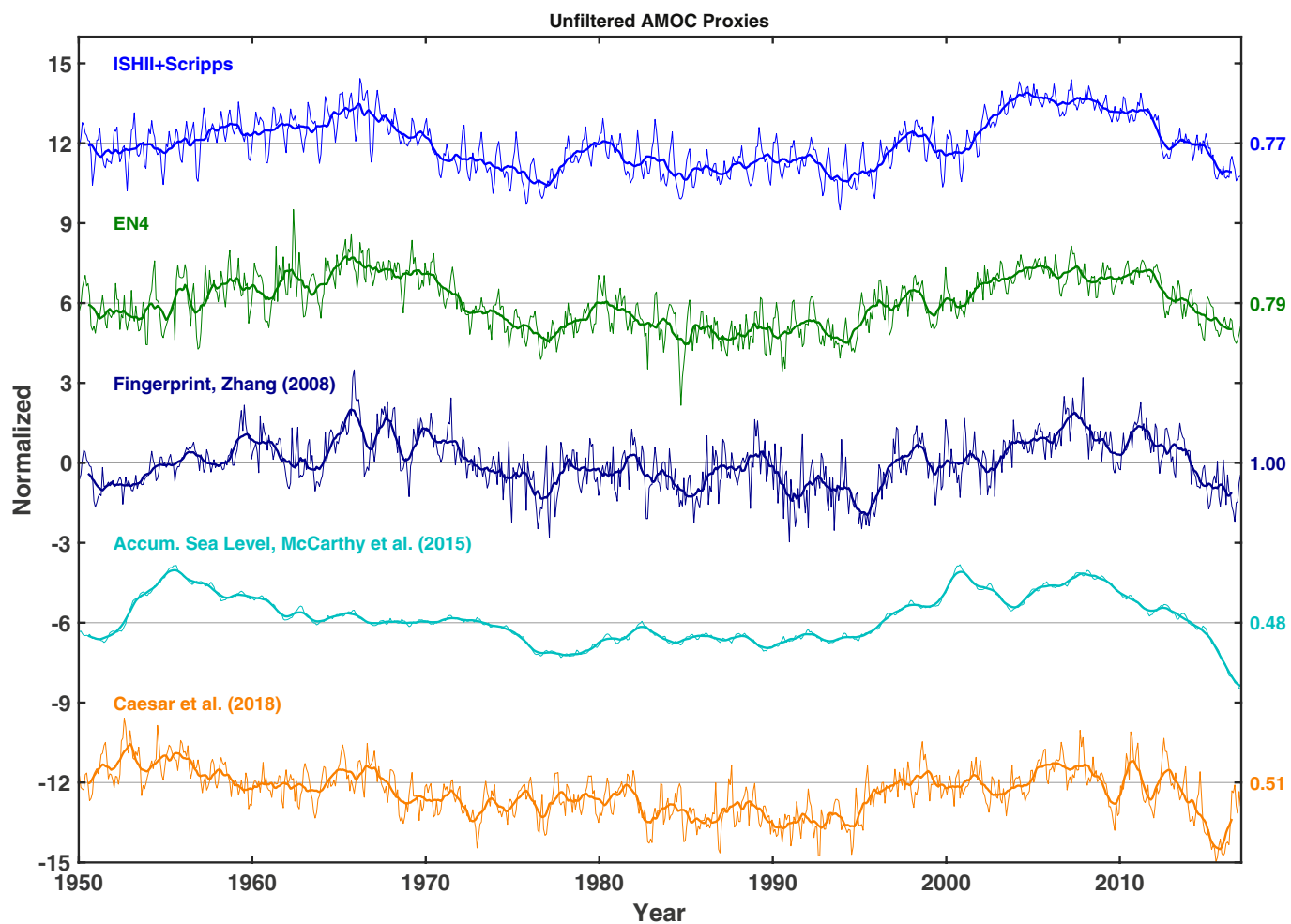
model preindustrial control runs, it seems that AMO is a surface manifestation of AMOC variation. Furthermore, based on palaeoclimate evidence of cold events when AMOC slows down abruptly, a common perception is that a slowdown in AMOC would lead to a cold Northern Hemisphere. The mechanism relies on the dominant role of AMOC (and its Gulf Stream) in horizontally transporting surface heat from the tropics to the mid- and high-latitude Atlantic, where it releases some heat to the cold atmosphere before sinking in the subpolar Atlantic. The heat released to the atmosphere makes Europe warmer (when wind blows in that direction) than it should be for its latitude.

Calculating SSH* from altimetry data. SSH* is SSH with its global mean subtracted. SSH contains both the thermosteric part (due to thermal expansion of the entire water column) and the ocean water mass addition that is due to melting land ice. It is known that the ocean will adjust to any change in ocean mass rapidly through the propagation of gravity waves, and will reach a new equilibrium globally within a couple of months³⁷. Therefore, the subtraction of the global mean largely removes the mass contribution from SSH.

Data availability. The datasets used in this study are all publicly available. They are: (1) ISHII data version 6.13, the objectively analysed subsurface temperature and salinity at 24 levels in the upper 1,500 m during 1945–2012 (<http://rda.ucar.edu/datasets/ds285.3/>); (2) Scripps gridded Argo data, objectively analysed subsurface temperature and salinity at 58 levels in the upper 1,950 m since 2004 (http://www.argo.ucsd.edu/Gridded_fields.html), which is based on Argo data collected and made freely available by the international Argo project and the national programmes that contribute to it; Argo float data and metadata are available from the Argo Global Data Assembly Centre (<https://doi.org/10.17882/42182>); (3) EN4 data version 4.2.1, objectively analysed subsurface temperature and salinity at 42 levels in the upper 5,350 m since 1900 (<https://www.metoffice.gov.uk/hadobs/en4/download-en4-2-1.html>); (4) Sea surface height based on satellite altimetry from the Archiving, Validation, and Interpretation of Satellite Oceanographic Data (AVISO) (<https://www.aviso.altimetry.fr/en/data.html>); (5) Tide gauge records from the Permanent Service of Mean Sea Level (PSMSL) (<http://www.psmsl.org>); (6) Extended Reconstructed Sea Surface Temperature (ERSST, version 3b) (<http://www1.ncdc.noaa.gov/pub/data/cmb/ersst/v3b/netcdf>); (7) RAPID AMOC at 26.5° N (http://www.rapid.ac.uk/rapidmoc/rapid_data/); (8) Ref.¹⁸, updated by the author (<ftp://oceancs-ftp.jpl.nasa.gov/pub/jwillis/AMOC/2016/>).

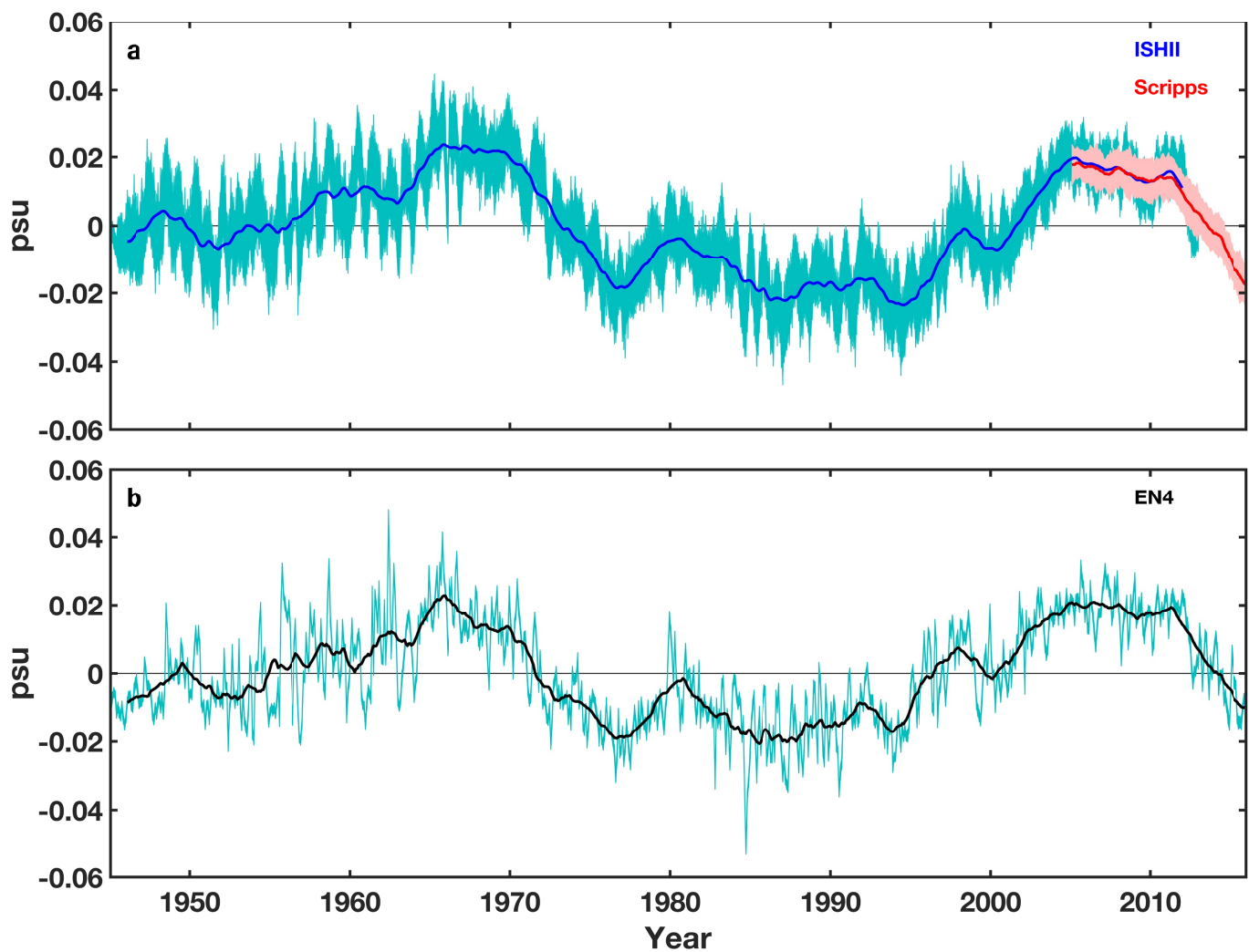
Code availability. Scripts for analysing the data are available from the corresponding author upon reasonable request.

31. Danabasoglu, G. et al. North Atlantic simulations in coordinated ocean-ice reference experiments phase II (CORE-II). Part II: interannual to decadal variability. *Ocean Model.* **97**, 65–90 (2016).
32. Saba, V. S. et al. Enhanced warming of the Northwest Atlantic Ocean under climate change. *J. Geophys. Res. Oceans* **121**, 118–132 (2016).
33. Zhang, R. & Vallis, G. K. The role of bottom vortex stretching on the path of the North Atlantic Western Boundary Current and on the North Recirculation Gyre. *J. Phys. Oceanogr.* **37**, 2053–2080 (2007).
34. Enfield, D. B., Mestas-Nunez, A. M. & Trimble, P. J. The Atlantic multidecadal oscillation and its relation to rainfall and river flows in the continental U.S. *Geophys. Res. Lett.* **28**, 2077–2080 (2001).
35. Delworth, T. L. & Mann, M. E. Observed and simulated multidecadal variability in the Northern Hemisphere. *Clim. Dyn.* **16**, 661–676 (2000).
36. Zhou, J., Tung, K. K. & Li, K.-F. Multidecadal variability in the Greenland ice-core records obtained using Intrinsic Time-scale Decomposition. *Clim. Dyn.* **47**, 739–752 (2016).
37. Lorbacher, K., Marsland, S. J., Church, J. A., Griffies, S. M. & Stammer, D. Rapid barotropic sea level rise from ice sheet melting. *J. Geophys. Res.* **117**, (2012).

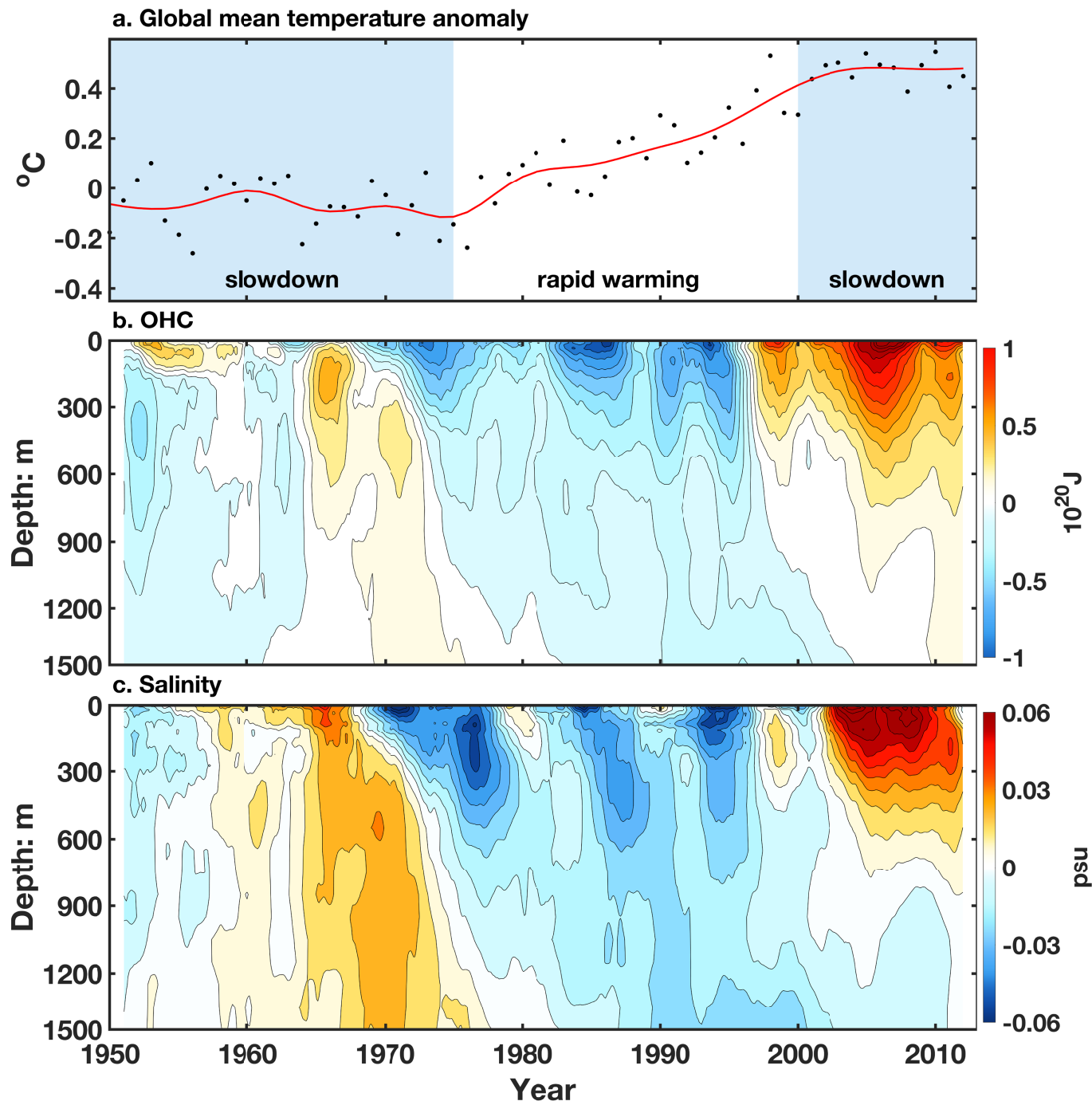


Extended Data Fig. 1 | Unfiltered AMOC proxy time series in monthly resolution. The thick solid lines are 13-month running means. The numbers to the right of each time series show the correlation coefficient with the unfiltered AMOC subsurface temperature fingerprint of Zhang.

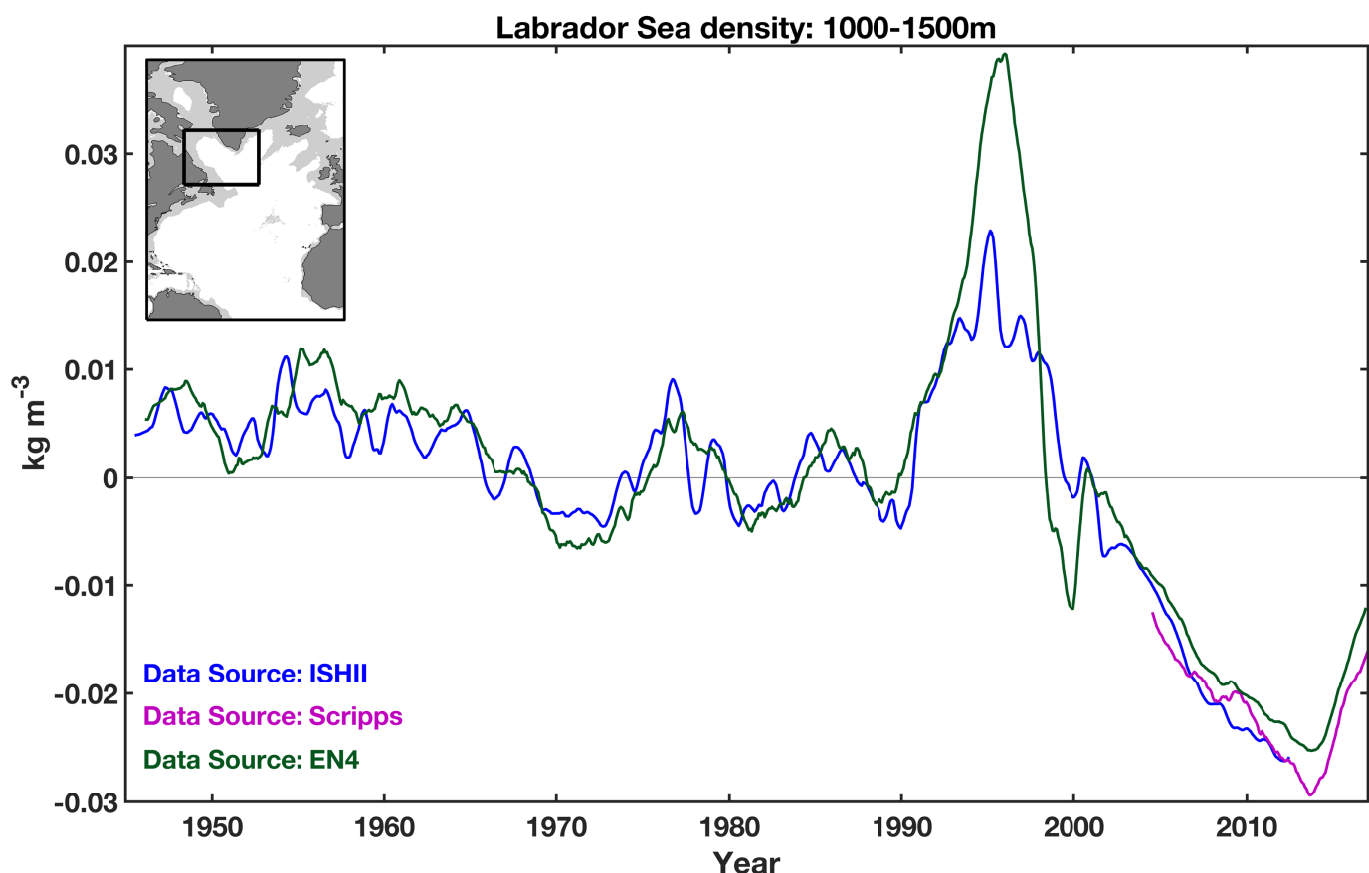
Data are taken from refs^{20–22}. All of the correlation coefficients are above 95% confidence level. The accumulated sea-level index is shifted to the right by 4.8 years in this figure. Without the time shift, its correlation with the AMOC proxy is practically zero ($r = 0.06$).



Extended Data Fig. 2 | Error bars for the three salinity time series shown in Fig. 1. The colour lines are monthly values of uncertainty, superimposed on the 13-month means of the time series. psu, practical salinity units.

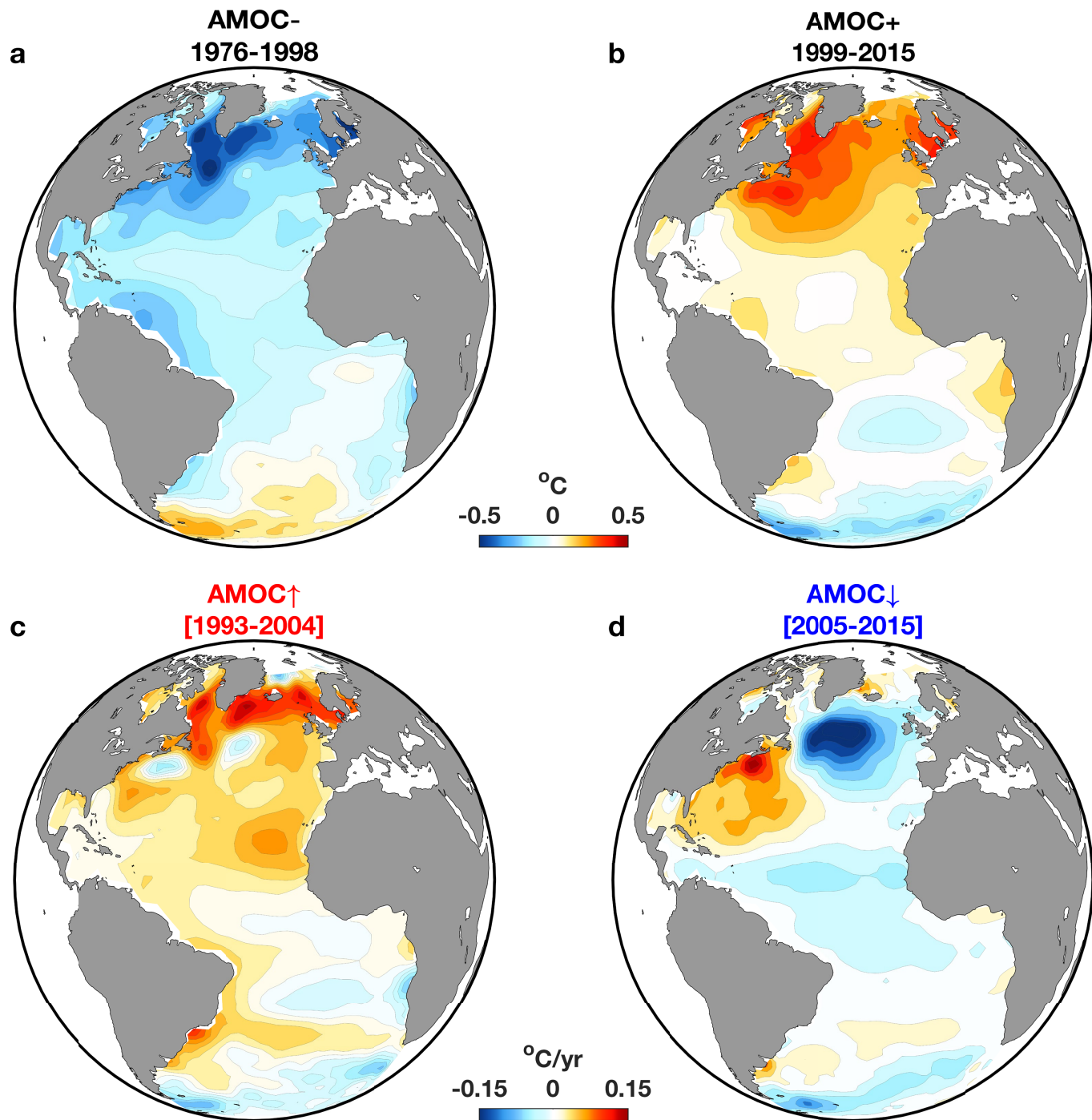


Extended Data Fig. 3 | Coincidence of the three AMOC phases with global warming slowdown and acceleration. **a**, Global mean surface temperature. **b**, OHC north of 45° N in the Atlantic. **c**, Salinity north of 45° N in the Atlantic.

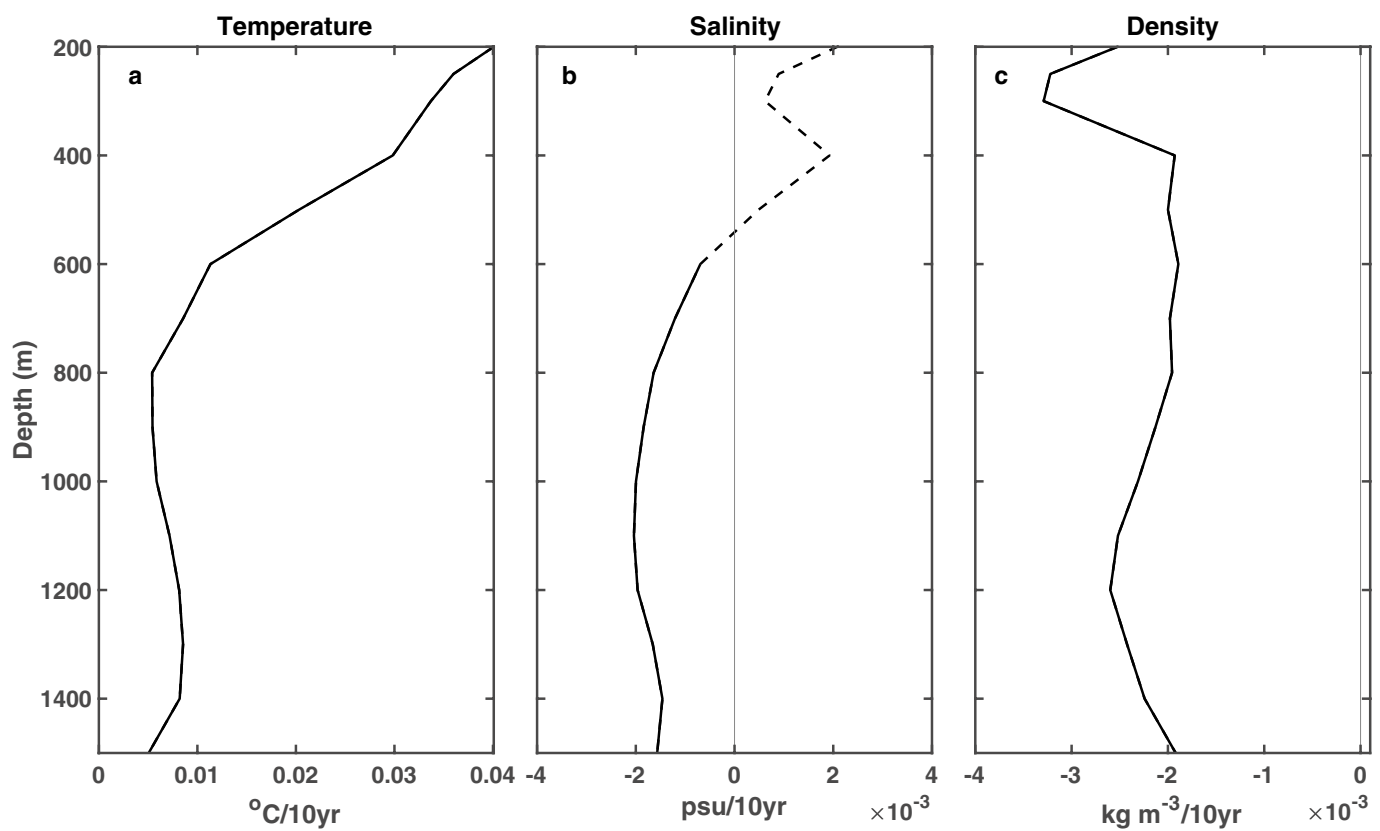


Extended Data Fig. 4 | Deep Labrador Sea density: Average density in the 1,000–1,500 m layer of the Labrador Sea, regionally averaged over the ocean area shown in the inset, from the three data sources given. A leading signal for stronger AMOC is the increased deep Labrador Sea salinity

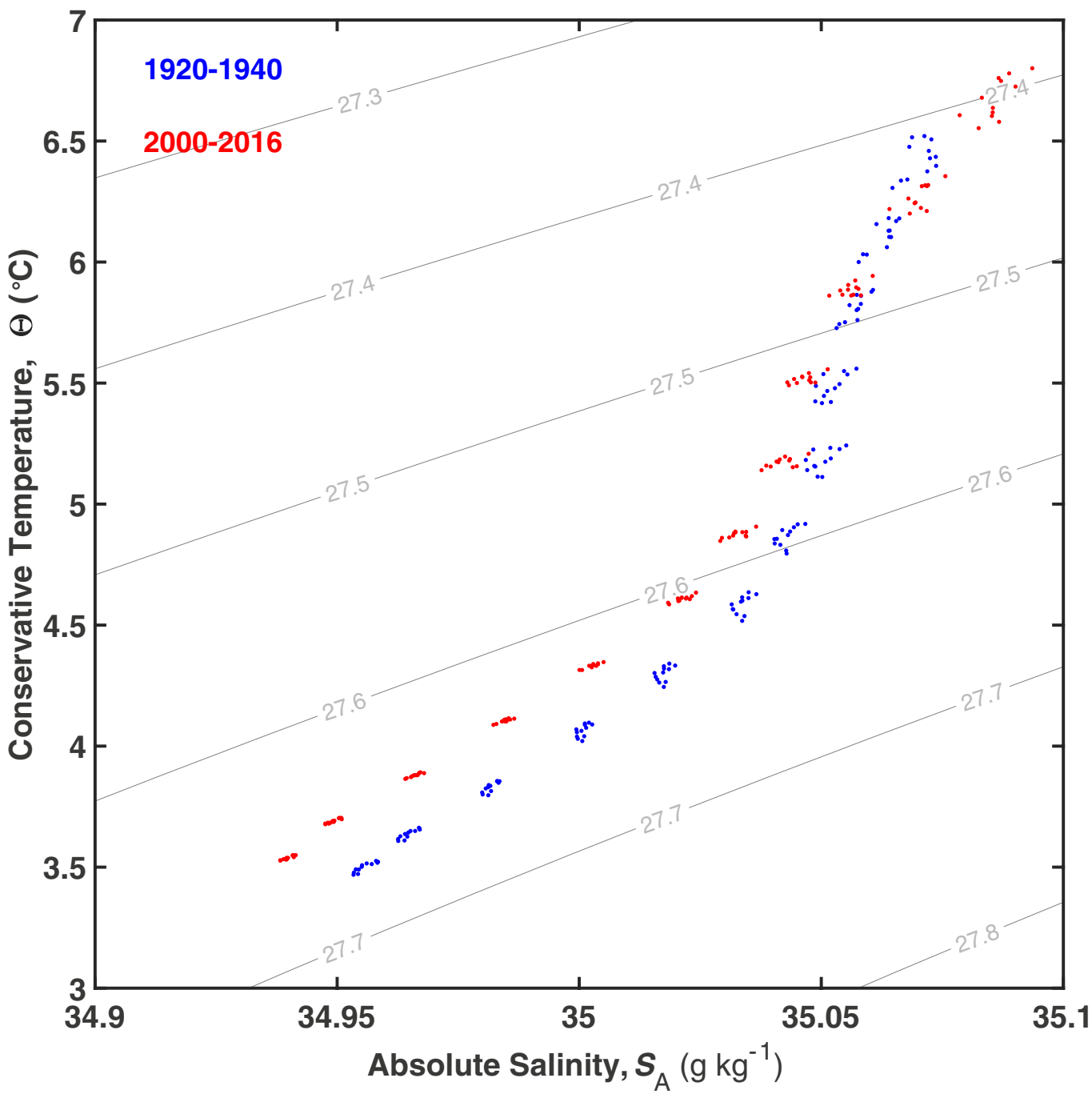
(and hence density). The signal propagates southward along the western boundary at depth, changing the cross-basin zonal gradient, and hence the geostrophic southward velocity¹³. The return flow then strengthens the upper branch of AMOC with a lag of 7–10 years^{15,16}.



Extended Data Fig. 5 | SST patterns during different AMOC phases. **a**, When AMOC is below climatology. **b**, When AMOC is above climatology, SST detrended. **c**, SST linear trend when AMOC is increasing. **d**, When AMOC is decreasing.



Extended Data Fig. 6 | Linear trends, from 1950 to 2017, of temperature, salinity and density. a–c, Trends in temperature (a), salinity (b) and density (c) as a function of depth. Solid curves indicate where the trend is statistically significant at 95% confidence level.



Extended Data Fig. 7 | Temperature–salinity diagram. The subpolar Atlantic Ocean (45° – 65° N) for each depth between 300 m and 1,500 m for the two periods, with the mean of 2000–2016 in red and the mean of 1920–

1940 in blue. The dots shown are the five winter month values (NDJFM). At these depths the seasonal cycle is very small³⁸.